

Report Title

Dipolar coupled nuclear spins for QIP

ABSTRACT

The goal of this project is to improve our control over nuclear spins in the solid state. We have:

1. Characterized the growth of multi-spin coherences in 1D and 3D spin systems under the dipolar interaction. Measured the decay rates of correlated spin states and characterized the resulting scaling behaviour.
 2. Studied the transport of polarization in 1D spin chains, both experimentally and in simulations. We have experimentally created states in which polarization is localized to the ends of the chain and studied the ensuing dynamics.
 3. Demonstrated the role of nuclear spin dipolar diffusion in dynamic nuclear polarization (DNP) experiments, in dielectric samples with abundant nuclear spins. Achieved a ^{29}Si polarization of 8.3% at 66 GHz and 1.1 K in single-crystal P-doped, the highest ever reported, using DNP. Took delivery of a He-3 cryostat that will allow these experiments to be extended to 94 GHz electron spin frequencies and 300 mK temperatures allowing us to achieve close to unit polarization.
-

List of papers submitted or published that acknowledge ARO support during this reporting period. List the papers, including journal references, in the following categories:

(a) Papers published in peer-reviewed journals (N/A for none)

1. Decay of highly-correlated spin states in a dipolar coupled solid, H. Cho, P. Cappellaro, D. G. Cory, C. Ramanathan, in press Phys. Rev. B. www.arxiv.org:cond-mat/0608620.
2. Solid state NMR three-qubit homonuclear system for quantum information processing: Control and characterization, J. Baugh, O. Moussa, C. A. Ryan, R. Laflamme, C. Ramanathan, T. F. Havel and D.G. Cory, Physical Review A, 73, 022305 (2006).
3. Single spin measurement using cellular automata techniques, C. A. Perez-Delgado, M. Mosca, P. Cappellaro and D. G. Cory, Physical Review Letters, 97, 100501 (2006).
4. Multi-spin dynamics of the solid state NMR free induction decay, H. Cho, T. D. Ladd, J. Baugh, D. G. Cory, C. Ramanathan, Physical Review B, 72, 054427 (2005).
5. Selective coherence transfers in homonuclear dipolar coupled spin systems, C. Ramanathan, S. Sinha, J. Baugh, T. F. Havel and D. G. Cory, Physical Review A, 71, 020303(R) (2005).
6. On the hydrodynamic approach to coherent nuclear spin transport, D. Greenbaum, M. Kindermann, C. Ramanathan and D. G. Cory, Physical Review B, 71, 054403 (2005).
7. Entanglement assisted metrology, P. Cappellaro, J. V. Emerson, N. Boulant, C. Ramanathan, S. L. Lloyd and D. G. Cory, Physical Review Letters, 94, 020502 (2005).
8. NMR quantum information processing, C. Ramanathan, N. Boulant, Z. Chen, D. G. Cory, I. Chuang and M. Steffen, Quantum Information Processing, 3, 15–44 (2004).
9. Spin diffusion of correlated two-spin states in a dielectric crystal, G. S. Boutis, D. Greenbaum, H. Cho, D. G. Cory and C. Ramanathan C, Physical Review Letters, 92, 137201 (2004).

Number of Papers published in peer-reviewed journals: 9.00

(b) Papers published in non-peer-reviewed journals or in conference proceedings (N/A for none)

Number of Papers published in non peer-reviewed journals: 0.00

(c) Presentations

Number of Presentations: 0.00

Non Peer-Reviewed Conference Proceeding publications (other than abstracts):

Number of Non Peer-Reviewed Conference Proceeding publications (other than abstracts): 0

Peer-Reviewed Conference Proceeding publications (other than abstracts):

Number of Peer-Reviewed Conference Proceeding publications (other than abstracts): 0

(d) Manuscripts

Single Nuclear Spin detection for the Read Out of Scalable NMR Quantum Computers, M. Kindermann and D. G. Cory, Quantum Information Processing, 2006, (submitted).

Number of Manuscripts: 1.00

Number of Inventions:

Graduate Students

<u>NAME</u>	<u>PERCENT SUPPORTED</u>	
Ka Yan Lee	0.33	No
Cecilia Lopez	0.49	No
Paola Capellaro	0.39	No
Jamie Yang	0.13	No
Murali Kota	0.08	No
HyungJoon Cho	0.28	No
Zhiying Chen	0.06	No
FTE Equivalent:	1.76	
Total Number:	7	

Names of Post Doctorates

<u>NAME</u>	<u>PERCENT SUPPORTED</u>	
Benjamin Levy	0.52	No
FTE Equivalent:	0.52	
Total Number:	1	

Names of Faculty Supported

<u>NAME</u>	<u>PERCENT SUPPORTED</u>	National Academy Member
David Cory	0.14	No
FTE Equivalent:	0.14	
Total Number:	1	

Names of Under Graduate students supported

<u>NAME</u>	<u>PERCENT SUPPORTED</u>
FTE Equivalent:	
Total Number:	

Names of Personnel receiving masters degrees

<u>NAME</u>	
Ka Yan Lee	No
Total Number:	1

Names of personnel receiving PHDs

<u>NAME</u>	
Paola Cappellaro	No
HyungJoon Cho	No
Murali Kota	No
Zhiying Chen	No
Total Number:	4

Names of other research staff

<u>NAME</u>	<u>PERCENT SUPPORTED</u>	
Chandrasekhar Ramanathan	0.43	No
Sergio Valenzuela	0.07	No
Timothy Havel	0.02	No
Peter Allen	0.45	No
FTE Equivalent:	0.97	
Total Number:	4	

Sub Contractors (DD882)

Inventions (DD882)

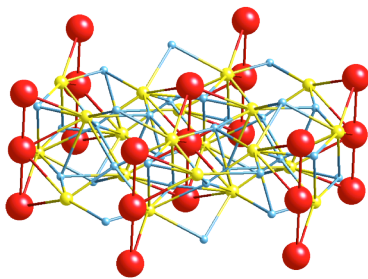
Scientific Progress (46940PHDRP)

The goal of this project is to improve our control over nuclear spins in the solid state.

1. We have characterized the growth of multi-spin coherences in 1D and 3D spin systems under the dipolar interaction. We also measured the decay rates of correlated spin states and characterized the resulting scaling behaviour.
2. We studied the transport of polarization in 1D spin chains, both experimentally and in simulations. We have experimentally created states in which polarization is localized to the ends of the chain and studied the ensuing dynamics.
3. We demonstrated the role of nuclear spin dipolar diffusion in dynamic nuclear polarization (DNP) experiments, in dielectric samples with abundant nuclear spins. We achieved a ^{29}Si polarization of 8.3% at 66 GHz and 1.1 K in single-crystal P-doped, the highest ever reported, using DNP. We recently took delivery of a He-3 cryostat that will allow these experiments to be extended to 94 GHz electron spin frequencies and 300 mK temperatures allowing us to achieve close to unit polarization.

Multiple quantum dynamics in extended spin networks

In solids it is possible to create states that show long-range correlations among the crystal spins, with a high degree of entanglement. The dynamics of these states have been studied in the spectroscopy literature for many years, but an exact understanding of the dynamics is precluded by its complexity. On the other end, an analytical solution for 1D models is possible using the fermionic operators, taking into account nearest-neighbor couplings only. The possibility to experiment on a quasi-1D system is therefore of particular interest to study the crossover from a pure 1D dynamics, which can be simulated classically in an efficient way, to a 3D dynamics, where an exact classical simulation is prohibited by the size of the Hilbert space of interest.



Fluoroapatite

The systems we use are calcium fluoride (CaF_2) and fluoroapatite (FAP). The fluorine spins in CaF_2 form a cubic lattice, while FAP presents linear chains of spins (nearest-neighbor spacing 3.44 Å) separated by an inter-chain distance of 9.37 Å. The chains appear isolated at short times, but inter-chain effects become important at longer times. By orienting the crystal in the magnetic field it is possible to quench or enhance the inter-chain couplings, thus allowing us to explore different

regimes and the transition from 1D to 3D dynamics.

One of the simplest experiments in many-body dynamics is the solid state NMR free induction decay. Following a $\pi/2$ pulse applied to spins in equilibrium in an external field, the observed signal decays. This decay results from the transformation of the observable single-spin single-quantum terms in the density matrix to multi-spin single quantum terms under the action of the dipolar interaction. We have recently developed

new multiple quantum encoding sequences that allow us to measure the growth of multi-spin correlations during evolution under the dipolar Hamiltonian. By performing a rotation about an arbitrary axis, it is possible to measure the distribution of coherence numbers in a basis in which the rotation axis appears to be the quantizing axis. Figure 2 shows the measured free induction decay of CaF_2 , as well as the distribution of multi-spin coherences measured at different times.

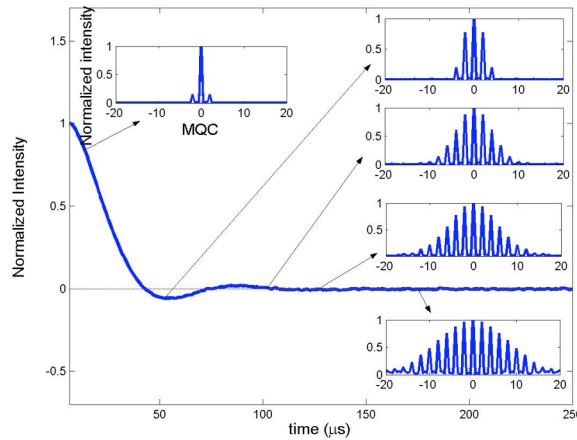


Figure 2. Growth of multiple spin correlations during the NMR FID in CaF_2

We plot the growth of multiple quantum intensities as a function of the dipolar evolution time in Figure 3. The growth of quantum coherences shows an initial oscillation between the zero and double coherence operators (which can be reproduced by a 2-spin model of the evolution) followed at later times by a sigmoidal growth of the higher coherence order. In the case of a linear spin chain, the oscillations (predicted by the fermionic solution) last longer, until next-nearest neighbors and later inter-chain interactions come into the play. As a consequence, the growth rate of higher coherences is much slower.

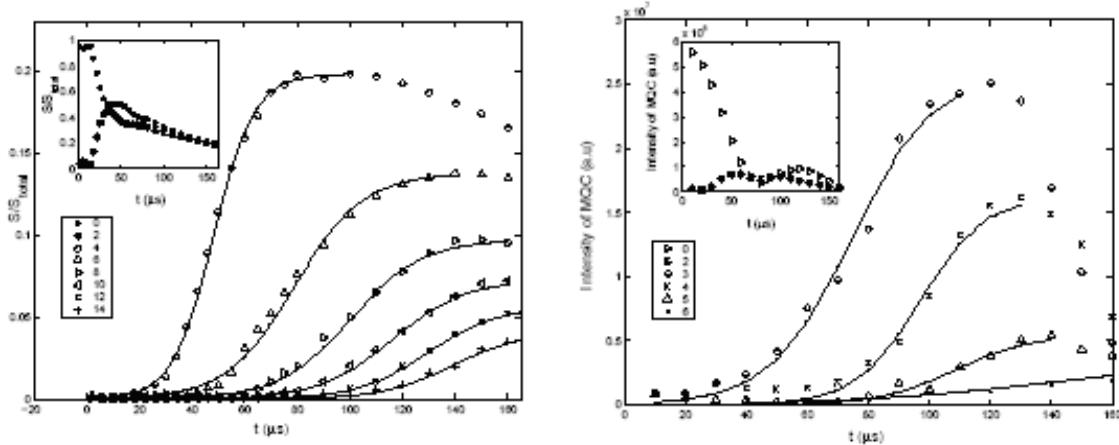


Figure 3. The growth of multiple spin correlations (normalized with respect to the total signal for that evolution time to compensate for imperfect refocusing) showing sigmoidal fit to the initial growth data of each coherence order. The insets show the dynamics of 0 and 2 coherence orders. Left: CaF_2 along the $[110]$ direction, Right: Fluorapatite.

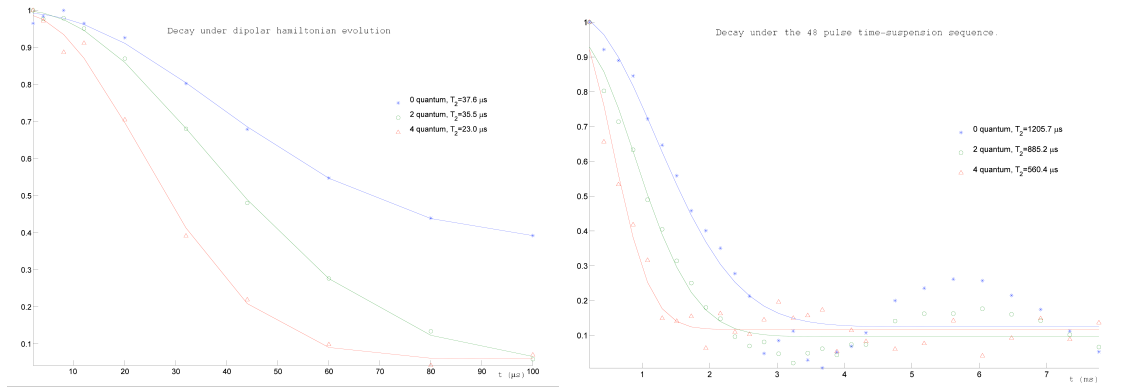


Figure 4. Decay of multiple quantum coherences in FAp during evolution under the internal dipolar Hamiltonian and during an NMR pulse sequences that averages the dipolar coupling to zero.

A similar slower dynamics is also observed in Figure 4 when we compare the decay of the signal from the different coherences under the evolution imposed by the dipolar Hamiltonian or unrefocused operators in the time-suspension sequence. This apparent decay is a consequence of the creation of more complex correlation among nuclear spins that can no longer be refocused to observable single spin operators in the following step. At short preparation times (indicated in the figure), there are relatively few spins in the correlated spins states, while at longer times there are significantly more correlated spins.

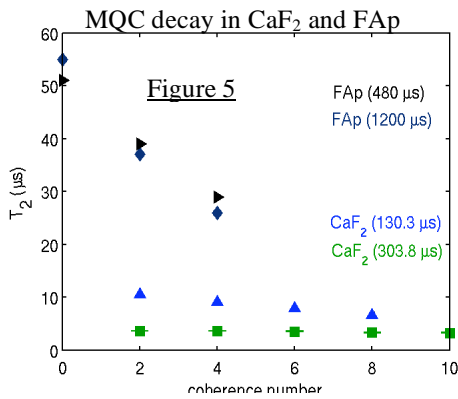


Figure 5 shows a comparison of the results on the 3D and 1D systems shows that the dynamics are much more restricted in a 1D system, and that the correlations are created on a longer time scale and the decay is observed to be much slower. Such comparisons between the dynamics of 3D and 1D systems will allow us to probe interesting question of where lies the threshold between systems that can be simulated efficiently classically and where a simulation on a quantum information processor becomes needed.

All the signals were observed to decay as Gaussian functions in time, and the characteristic decay time T_2 reported here was the standard deviation of the Gaussian. It is seen that T_2 depends both on the number of correlated spins N (via the preparation time), and on the coherence number n , and in fact appears to vary linearly with coherence number. For the CaF_2 system we were able to find a general relationship for the coherence time

$$T_2 = \frac{A}{\sqrt{N}} - \frac{B \cdot n}{N}$$

where A and B are constants. The same scaling law was observed when we attempted to refocus the dipolar evolution, using the time-suspension sequence.

Dynamics of 1D spin chains

One dimensional spin chains have been proposed as a bus to transfer information from one part of a quantum computer to another. The dynamics of a one dimensional spin chain with only nearest neighbor couplings of the form of an Ising, XY or double quantum Hamiltonian are exactly solvable. However, the spins in a real spin chain are coupled together via dipolar interactions, and no solution exists for this interaction.

An infinite linear chain of dipolar coupled spins is a highly symmetric system; if the only control available is an external radio-frequency field that acts collectively on all the spins, this symmetry cannot be broken and therefore only a small subspace of the total Hilbert space can be reached by the system during its evolution. If the spin chain is instead of finite length, the symmetry is naturally broken by the boundary conditions. The spins at the extremities of the chain only have one nearest neighbor to which they are strongly coupled. This implies a slightly different energy and also different dynamics under the internal dipolar hamiltonian with respect to the other spins. This evolution and the control Hamiltonians are still not enough for universal control, as it can be verified by calculating the rank of the Lie algebra generated by the internal and control Hamiltonian (this can be done numerically for small systems of 4-5 spins). However, it is possible to exploit this broken symmetry to create states, where the polarization is localized to the chain ends, and to then examine how this polarization is transported through the chain under the spin-spin couplings.

In the FAp system, the next-nearest neighbor coupling is a factor of 8 times smaller than the nearest neighbor couplings, and the coupling between spins on different chains is about a factor of 30 smaller than the nearest neighbor coupling. If we consider the short-time evolution only, the spin dynamics are dominated by the nearest neighbor interaction. However, at longer times, the longer range interactions lead to a deviation of the spin dynamics from the simple models.

Consider a single chain with a fixed number N of spins, which evolves unitarily under the dipolar hamiltonian and the external control rf field, and decoheres because of its interaction with the environment. The environment therefore also includes the effects of other chains and the distribution in chain composition. In the equilibrium thermal state $\Sigma_i \sigma_z^i$, the polarization is spread equally over the entire spin chain. The pulse sequence shown in Figure 6, combined with phase-cycling, can be used to prepare the initial state $\sigma_z^1 + \sigma_z^N$ from the thermal state. Note that in this state the polarization is stored only at the ends of the chain.

It is straightforward to understand how the sequence works. Following the first

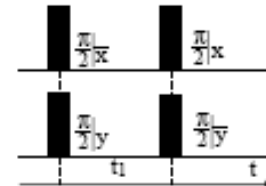


Figure 6

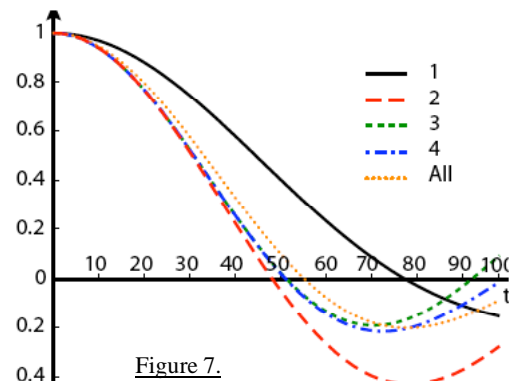


Figure 7.

$\pi/2$ -pulse, the dynamics of the end-chain spins is quite different from the dynamics of the internal spins in the chain. When we look at the polarization of individual spins by numerical simulations of 8-10 spin systems (Figure 7), we notice oscillations in polarization of each one of them. In particular the first and last spins have a much slower dynamics (apparent decay) at short time, which is due to the smaller number of couplings.

We can therefore select a time at which the state of the two end spins is still mainly σ_x , while all the other spins have evolved to more complex multi-body states. A second $\pi/2$ pulse will bring the magnetization of spins 1 and N to the longitudinal (z) axis, so that the density matrix describing the system can be written as $\sigma_z^1 + \sigma_z^N + \rho'$. For fluorapatite we found that the optimal time between $\pi/2$ pulses is $30.3\mu\text{s}$. Except for very short chains (3-4 spins), the optimal time between pulses is almost independent of the number of spins in the chain, therefore allowing us to choose the time even if we don't know the number of spins in a chain. To select only the desired (first two) terms, we cycle the pulses through different phases, thus averaging to zero all terms which are not either populations or zero quantum terms.

Figure 8 shows the experimentally obtained spectra for an initial thermal state and for the initial state with the polarization only at the chain ends. It is also possible to observe the signature of these initial states in the multiple quantum dynamics of the spin chain, as the system evolves under the double-quantum (DQ) Hamiltonian. The DQ Hamiltonian is exactly solvable for a 1D system with nearest neighbor couplings, so the experimental results can readily be compared to theory.

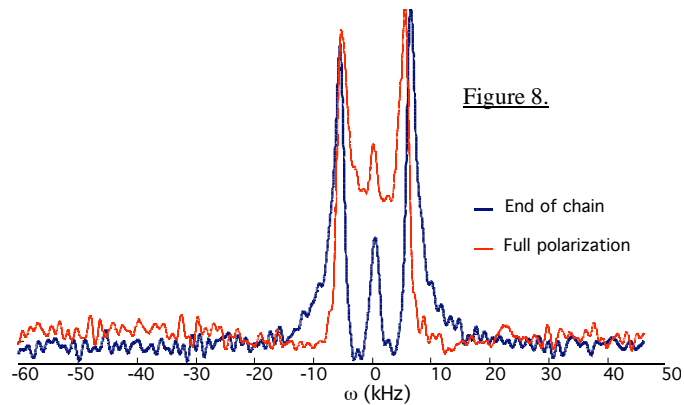


Figure 8.

Figure 9 shows the experimentally measured intensities of the zero and double quantum coherences for the collective thermal initial state (left) and the end-chain selective states (right), as well as the theoretically expected results for a spin chain of 11 spins (assuming nearest neighbor couplings). The agreement is seen to be excellent, indicating that we have indeed created a state with polarization only at the ends of the chain.

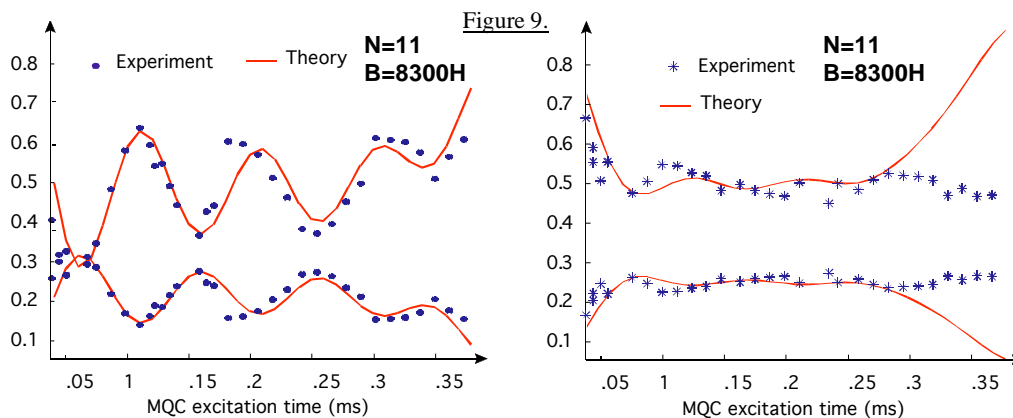


Figure 9.

Another interesting feature of the DQ Hamiltonian is its similarity to the XY Hamiltonian. Polarization transfer driven by the XY and DQ Hamiltonians yield the same result if the number of spins in the chain is odd. If we take the absolute value of the polarization, the two Hamiltonians produce the same transport of polarization and therefore the double-quantum Hamiltonian can be used to simulate the flip-flop Hamiltonian that is not available in the system. Figure 10 shows the results of simulations for the transport of polarization under the XY Hamiltonian for an initial state where the polarization is only stored on one end of the spin chain (note we cannot create this state experimentally as yet). The inset shows the transport under the XY and DQ Hamiltonians, showing the similarity between the two.

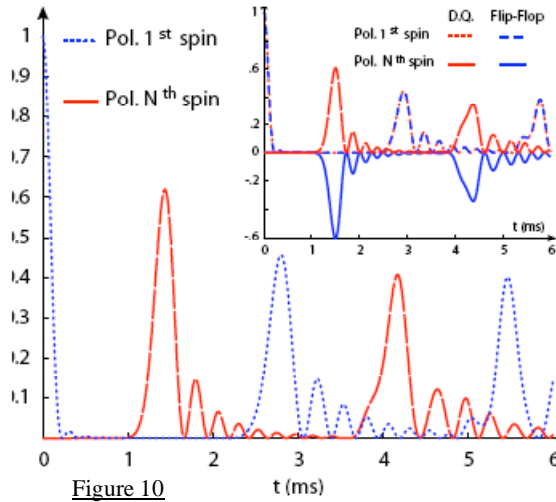


Figure 10

The transport of polarization cannot be detected directly (unless one introduces very strong magnetic field gradients, able to produce an appreciable change of frequency over distances of a few nanometers). It is however possible to monitor the MQC intensities to detect the occurred transfer of polarization. If one is therefore interested in the transfer of polarization from one end of the chain to the other it is possible to follow this transfer driven by the DQ Hamiltonian by measuring the multiple-quantum intensities. In Figure 11 we show how this transport and detection method would look like for our experimentally prepared initial state with polarization on both ends of the chain. Next-nearest neighbor couplings and cross-chain couplings offer additional pathways that can result in an acceleration of information transport, which has no classical counterpart. This transition from a behavior that can be simulated classically to the more complex quantum behavior is of tantamount importance in the context of QIP, where the efficiency of a quantum computation is brought by the coherence and interference effects proper of quantum mechanics.

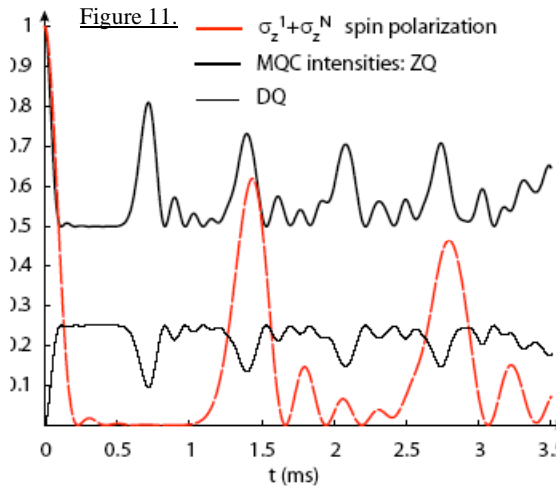


Figure 11.

Dynamic Nuclear Polarization (DNP)

At room temperature, the nuclear spins are infinitesimally polarized ($\sim 10^{-5}$) in laboratory magnetic fields, and the spin system is highly mixed. As the Zeeman energies are very small the spins remain highly mixed even at liquid helium temperatures. It is necessary to cool the sample to milliKelvin temperatures in order to achieve significant polarization. Alternatively, the spin system can be highly polarized by techniques such as dynamic nuclear polarization which involves polarization transfer from electronic spins, mediated by the hyperfine interaction. The increased polarization will allow us to explore systems with a larger number of qubits, and also allows preparation of the system close to a pure state.

Our DNP setup operates at a field of 2.35T, which corresponds to an electron Larmor frequency around 66 GHz for $g=2$. The system uses a Bruker Avance NMR spectrometer with a home-built probe, containing a horn antenna for the microwaves, and a solenoidal RF coil (Figure 12).

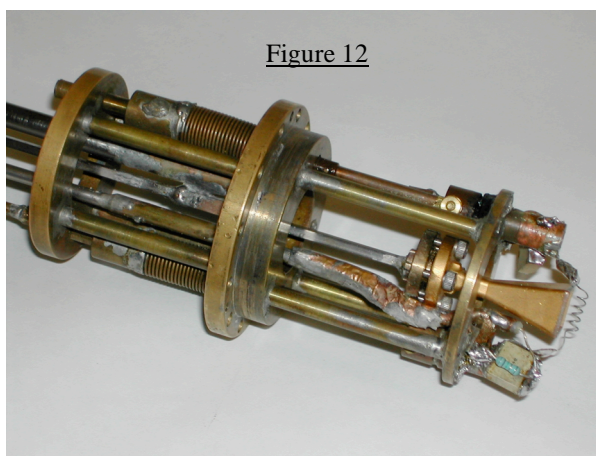
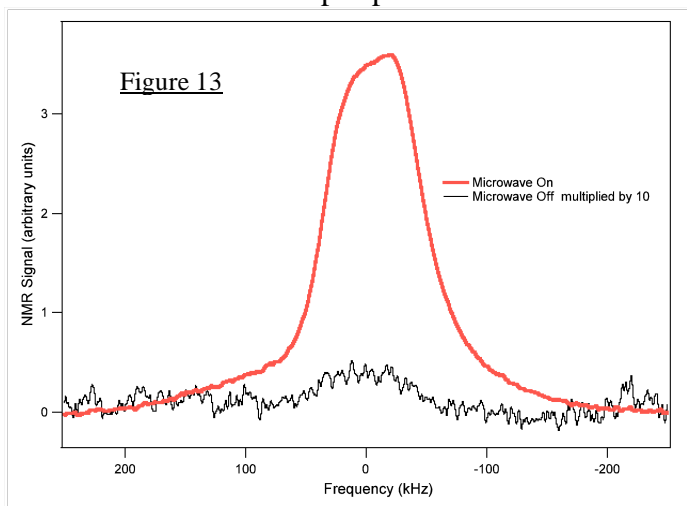


Figure 13 shows the NMR spectra of the water-glycerine sample, illustrating a ^1H signal enhancement of 70 produced by dynamic nuclear polarization (DNP) at 1.40 K. The sample consisted of 40 mM of nitroxide TEMPO dissolved in a 40:60 water:glycerol mixture. The top spectrum was obtained after irradiating the sample with microwaves at 65.9 GHz for 53 minutes. The estimated nuclear spin polarization in this experiment was about 12%. The bottom spectrum was obtained under the same conditions but without microwave irradiation. The frequency shift is relative to 100.13 MHz. The enhancement over the room temperature polarization is about 15000. The polarization of the $g=2$ electron spins is 81 % under these conditions. The microwave source used was a 60 mW Gunn diode source (Millitech).

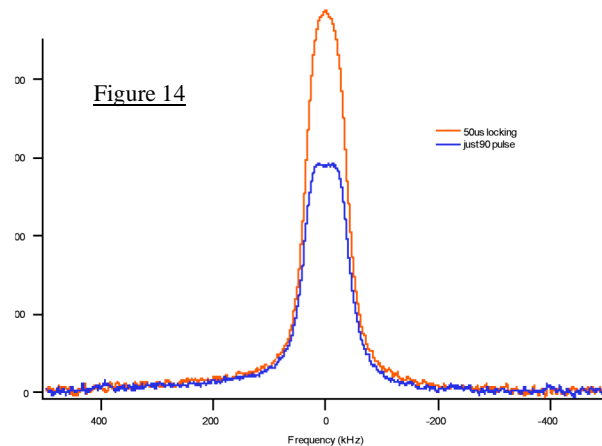


DNP and dipolar diffusion

In the DNP process the initial enhancement is local to the site of the paramagnetic impurity (the electron spin). In order to polarize a bulk nuclear spin system, this process needs to be repeated many times, and the non-equilibrium polarization transported away from the site of the impurity to the bulk. This process is mediated by spin diffusion and is essentially the inverse of the standard T_1 relaxation mechanism in dielectric solids. Spin diffusion is the process by which polarization is transported through a lattice of spins, mediated in most cases by the XY or flip-flop terms of the dipolar interaction. In a high magnetic field, the Zeeman energy and the dipolar energy of the spins are both independently conserved, and have different diffusion and spin-lattice relaxation rates.

In the traditional model, the spins in an inner core around the impurity are essentially frozen in place. They experience a significant local field due to the impurity, and as a consequence they have significantly different Zeeman energies. This energy difference suppresses the XY interaction, creating the so-called "spin-diffusion barrier" around the impurity. In order to transfer polarization across the barrier, an additional source of energy is needed to make up the energy difference between the spins. The nuclear spin dipolar reservoir provides this energy that permits the polarization to cross the barrier. Thus at the site of the impurities the Zeeman and dipolar reservoirs are seen to mix. Once past the spin diffusion barrier, the polarization is transported across the crystal via Zeeman spin diffusion. However, we have recently shown that the diffusion of dipolar order is significantly faster than that of Zeeman order, so the cooling of the dipolar reservoir that is produced locally at the spin diffusion barrier, should quickly be communicated to the bulk. We would therefore expect the effective spin temperature of the bulk dipolar reservoir to be significantly lower than that of the Zeeman reservoir.

Figure 14 shows the signal obtained following a $\pi/2$ pulse, and following a 50 μs spin locking pulse with a weak RF. As this field is comparable to the strength of the local proton dipolar field in the sample, it induces mixing between the Zeeman and dipolar reservoirs. The additional signal enhancement obtained following this mixing indicates that the bulk dipolar reservoir has a lower effective spin temperature than the Zeeman reservoir following microwave irradiation. In fact, given the much smaller heat capacity of the dipolar bath compared to the Zeeman bath at high magnetic fields, the effective temperature of the dipolar system is much colder than that of the



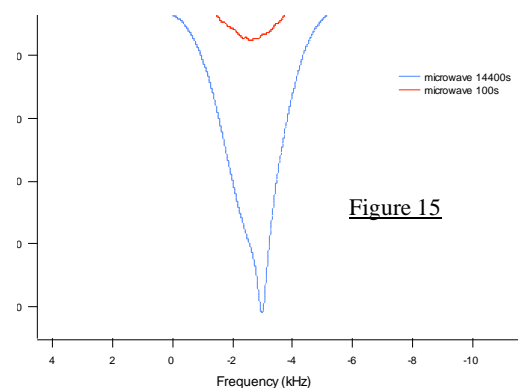
Zeeman system. At long times, we would expect the temperatures of the two reservoirs to once again become equal.

We suggest that it is the difference in the spin diffusion rates of the Zeeman and dipolar order that is responsible for the difference in the effective spin temperatures at short times. The faster dipolar diffusion allows a faster cooling of this reservoir. A similar cooling of the dipolar reservoir has also been observed following optical pumping of semiconductor systems such as GaAs and InP. It should be possible to polarize a sample more rapidly by repeatedly cooling the dipolar reservoir and transferring this polarization to the Zeeman reservoir. This transfer could be done adiabatically using an adiabatic remagnetization in the rotating frame (ARRF). Note that this transfer of order occurs in the bulk crystal, not just locally to the sites of the defects.

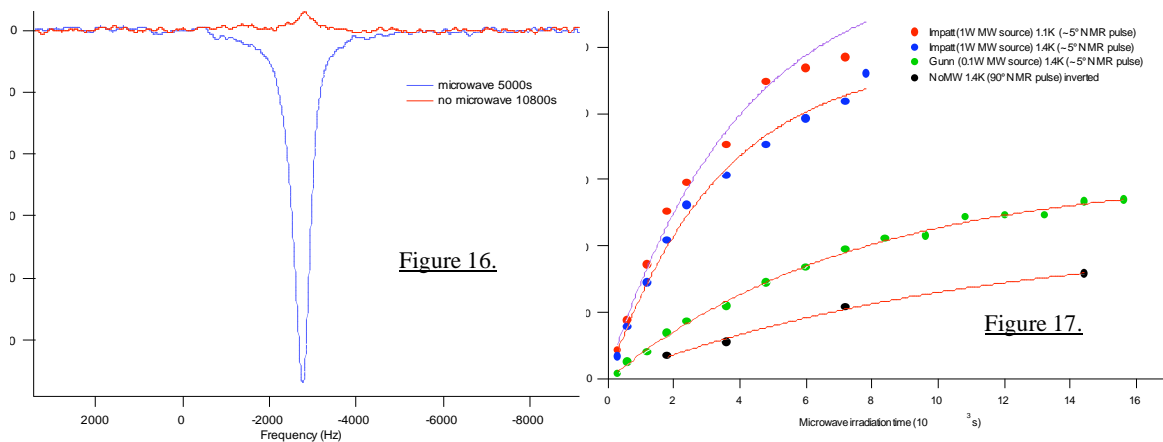
Silicon DNP

Patterned ^{29}Si (spin $1/2$) structures on a ^{28}Si (spin 0) substrate are promising for spintronics in general and spin-based quantum computing. Polarizing silicon spins is therefore of significant interest. Here we show the use of DNP to polarize ^{29}Si spins. The electron magnetic moment is about 3500 times larger than the nuclear magnetic moment of ^{29}Si .

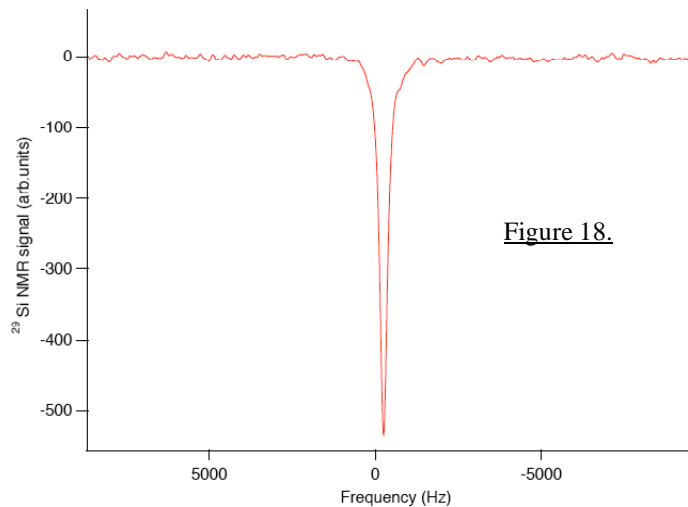
We performed DNP experiments on a commercially obtained sample of powdered silicon, and a variety of single crystal samples doped with antimony or phosphorus of varying concentrations. The natural abundance of ^{29}Si in these samples is 4.7 %. Figure 15 shows the DNP enhancement for a sample of Si powder obtained from Alfa Aesar with 99.999% purity (1-5) μm particles. The ESR signal primarily arises from dangling bonds on the surface of the Si particles in this case. The Si polarization obtained was 5%. The experimental setup was identical to that used in the TEMPO experiments above, except that the RF coil was tuned to silicon.



We also performed DNP experiments on antimony (Sb) and phosphorus (P) doped single crystals of silicon. Figure 16 shows the NMR signal from a single crystal of Si doped with Sb at a concentration of $3 \times 10^{17} \text{ cm}^{-3}$. Figure 17 shows the growth of the DNP enhanced signal as a function of the microwave irradiation time, and as a function of microwave power. We used a 100 mW Gunn source, and a 1 W custom-built source from Quinstar Technologies. The 1 W source consists of 2 Impatt diode sources, both injection locked with a Gunn in order to reduce the phase noise, whose outputs are combined. The data seems to indicate that the B_1 field at the site of the spins is still too low to efficiently drive the DNP process.



We replaced the horn antenna with a cylindrical TE_{011} resonator in order to increase the cavity Q and hence the B_1 field produced, and performed DNP experiments on a new sample of P-doped Si wafers with a doping concentration of $2 \times 10^{17} \text{ cm}^{-3}$. We also setup a Roots blower to pump the helium space and lower the temperature in our cryostat to 1.1 K. This increases the electron spin polarization to 89%. Figure 18 show the ^{29}Si spectrum from this sample after microwave irradiation of the sample at 65.86 GHz for 2 hours. During irradiation the sample was placed inside the cylindrical cavity and was subsequently moved to rf coil outside of the cavity for detection. The maximum DNP enhancement obtained was about 200, corresponding to the nuclear spin polarization of 8.3%. The frequency shift is relative to 19.89 MHz.



He-3 system

We have now received our helium-3 cryostat that will allow us to perform DNP experiments at temperatures down to 300 mK. The cryostat fits into a custom-designed bucket dewar containing a variable-field NMR quality superconducting magnet that can reach fields of up to 4.2 T. We have an injection-locked Impatt diode source capable of delivering 500 mW of power at 94 GHz. The lower temperatures and higher fields accessible with this system will allow us to achieve significantly higher polarizations than those described above.

Figure 19 schematically illustrates the experimental arrangement. The sample is immersed in helium-3 in order to ensure that it is thermally sunk to the lowest temperature possible. The microwave and RF components are heat-sunk to 4 K. A silver-plated stainless steel waveguide is used to transmit microwave power from the Impatt diode source to the Fabry-Perot cavity in which the sample is placed. A piezo-electric motor allows us to accurately position the mirror and maintain cavity tuning as the system is cooled.

In addition to the lower temperatures and higher microwave powers accessible with this system, a significant advantage of this system is the variable-field superconducting magnet. This will allow us to explore a variety of electron spin defects in materials with different g-factors.

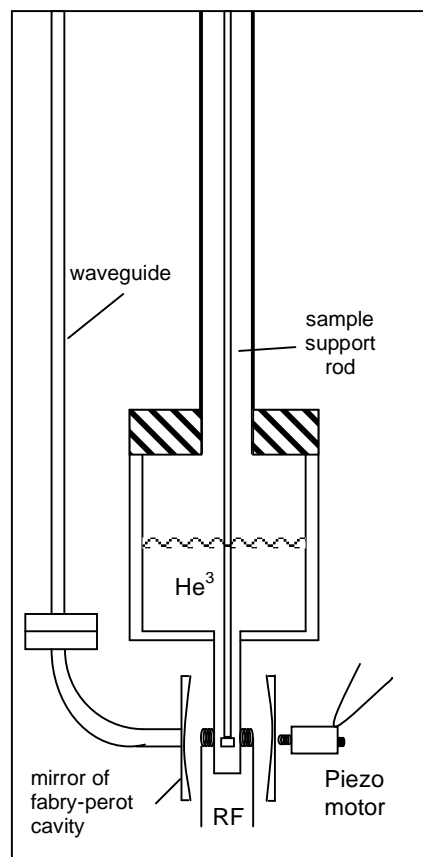


Figure 19.